Experimental demonstration of a hybrid III–V-on-silicon microlaser based on resonant grating cavity mirrors

Yannick de Koninck,[1,*] Fabrice Raineri,[2,3] Alexandre Bazin,[2] Rama Raj,[2] Gunther Roelkens,[1] and Roel Baets[1]

[1]*Department of Information Technology, Photonics Research Group, Ghent University—imec Center for Nano- and Biophotonics (NB-photonics), Sint-Pietersnieuwstraat 41, B-9000 Ghent, Belgium*

[2]*Laboratoire de Photonique et de Nanostructures, CNRS-UPR20, Route de Nozay, 91460 Marcoussis, France*

[3]*Université Paris Denis Diderot, 75205 Paris, France*

**Corresponding author: yannick.dekoninck@intec.ugent.be*

Received April 22, 2013; revised June 10, 2013; accepted June 12, 2013;
posted June 14, 2013 (Doc. ID 188866); published July 10, 2013

We present the experimental demonstration of a novel class of hybrid III–V-on-silicon microlasers. We show that by coupling a silicon cavity to a III–V waveguide, the interaction between the propagating mode in the III–V waveguide and the cavity mode in the silicon resonator results in high, narrowband reflection back into the III–V waveguide, forming a so-called resonant mirror. By combining two such mirrors and providing optical gain in the III–V wire between these two mirrors, laser operation can be realized. This optically pumped device measures 55 by 2 μm, requires microwatt-level threshold pump power, and shows single-mode laser emission with a side-mode suppression ratio of up to 39 dB. © 2013 Optical Society of America

OCIS codes: (130.0250) Optoelectronics; (140.3948) Microcavity devices; (140.5960) Semiconductor lasers; (250.5960) Semiconductor lasers.
http://dx.doi.org/10.1364/OL.38.002496

Over the past decade, silicon photonics has emerged as a major technology platform for photonic integrated components and circuits. To add active functionality, one of the most promising approaches is the heterogeneous integration of III–V materials on the silicon die [1]. Distributed Bragg reflector and distributed feedback lasers have been demonstrated on this platform [1,2] using an evanescent gain scheme. This yields single-mode devices with high optical output, but the structures are large and require a fairly high threshold current (>20 mA). One way to reduce the threshold current is to scale down the size of the laser. Examples are III–V microdisk lasers [1], III–V photonic-crystal cavity lasers [3], and photonic crystal mirror VCSEL lasers [4]. The threshold pump power for these aforementioned microlasers is of the order of 1 mW or less. The lasing wavelength in these devices is determined either by the III–V processing or by the bonding layer thickness. In this Letter, we present the experimental demonstration of a novel hybrid III–V-on-silicon microlaser. The proposed device is small, resulting in low threshold pump power, and offers intrinsic single-mode laser operation. Moreover, the most critical device features are in the silicon layer, loosening the lithography and etching requirements in the less mature III–V technology.

The proposed design consists of two reflectors with the active laser cavity between. The laser cavity is a III–V waveguide with no silicon structures underneath, so in this part of the laser the light is fully confined to that III–V waveguide. In each of the two mirror sections there is a silicon cavity underneath the III–V wire. Such a cavity can, for example, be a grating waveguide with a quarter-wavelength phase shifting section in the center to support a localized defect resonance [5]. The interaction between the guided waveguide mode in the III–V wire and the localized resonance in the silicon cavity underneath will result in high, narrowband reflection back into the III–V waveguide; hence the name *resonant mirror*. Figure 1(a) shows a schematic side view of the laser. Light is generated and amplified in the III–V wire. As the light approaches the end of the III–V wire [1 in Fig. 1(a)], a small part of the light couples to the silicon cavity underneath (2). For wavelengths close to the silicon cavity resonance wavelength, power will build up inside the silicon cavity. Eventually the energy stored in the silicon cavity is high enough that a significant amount of optical power will couple back into the III–V wire. The light coupling back codirectionally to the incident light (3) will interfere destructively with the latter, resulting in zero transmission (4). On the other hand, the light coupling back counterdirectionally to the incident light (2) will provide feedback into the III–V wire (5), which is required in order to establish laser operation. Light can easily be extracted to a silicon output

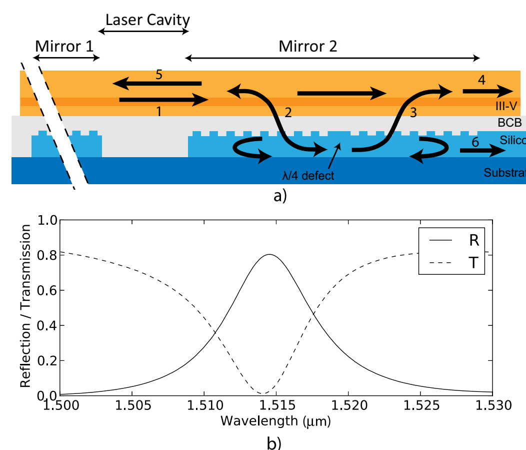

Fig. 1. (a) Schematic side view of the operation of the resonant mirror laser. (b) Reflection (R) and transmission (T) spectrum of resonant mirror with 285 nm grating period.

 © 2013 Optical Society of America

waveguide by tapping a small amount of the power built up in the silicon cavity to an external waveguide (6). A cavity coupled to the laser mesa to serve as a narrowband reflector was used in the past to reduce the laser linewidth [6]. More recently, the same principle was also used to design narrowband passive optical filters [7].

Because the power buildup only occurs close to the silicon cavity resonance wavelength, the reflection bandwidth of this type of mirror is relatively narrow (<10 nm). Since the reflection of such a mirror can be very high and the laser mode is confined to the III–V wire, which maximizes the modal gain, the length of the III–V wire can be reduced to make sure only one longitudinal resonance of the III–V cavity lies within the reflection bandwidth of the mirror, yielding an intrinsically single-mode laser with a short length. An in-depth theoretical treatment of resonant mirror lasers can be found in [5].

Figure 1(b) shows the reflection and transmission spectrum of a resonant mirror simulated by using a 3D finite-difference time-domain method. In this particular mirror, the silicon cavity is a 1.6 μm wide, 220 nm high strip waveguide with 70 nm deep periodic grating corrugations. It consists of 60 periods (285 nm period pitch) with a quarter-wavelength defect in the middle to support a resonance near the grating's Bragg wavelength. The III–V wire above is 1.6 μm wide and consists of an 80 nm thick InGaAsP (Q1.55) bulk active layer, sandwiched between two InP cladding layers of 10 nm (below InGaAsP) and 120 nm (above InGaAsP). The vertical spacing between the silicon layer and III–V layer is 240 nm.

The simulated spectrum in Fig. 1(b) shows that, at the silicon cavity's resonance wavelength (1514 nm), the structure reflects 80% of the incoming power back into the III–V waveguide. At that same wavelength, virtually no power (1.2%) is transmitted through the III–V waveguide. Most of the remaining 18% is directed to the output silicon waveguide. The full-width at half-maximum bandwidth of the reflection peak is 7 nm.

The optimal distance between the two mirrors in the laser configuration is determined by the reflection bandwidth of the mirror. To guarantee single-mode operation, the FSR of the laser's longitudinal modes should be at least of the order of the reflection bandwidth (7 nm), so the spacing between the mirrors should be sufficiently small. On the other hand, this mirror's peak reflectivity is only 80%, so the III–V waveguide should be sufficiently long to ensure that laser threshold can be reached with a reasonable pump power. Considering these two conditions, calculations show [5] that a good value for the spacing between the silicon mirrors is 20 μm, resulting in a laser cavity FSR of around 6 nm.

The device was fabricated starting from a silicon-on-insulator (SOI) die processed in a 200 mm pilot line through the ePIXfab multiproject wafer service [8] and a 210 nm thick III–V stack on an InP substrate. The composition of the III–V stack is as described above. The SOI die and the III–V die are bonded together using divinyl siloxane bis-benzocyclobutene (DVS-BCB) adhesive bonding [1]. The resulting spacing between the top of the SOI waveguide layer and the bottom of the III–V stack measures 240 nm ($200\ \mathrm{nm}\ SiO_2 + 40\ \mathrm{nm}$ DVS-BCB). After removing the InP substrate, the III–V mesa is

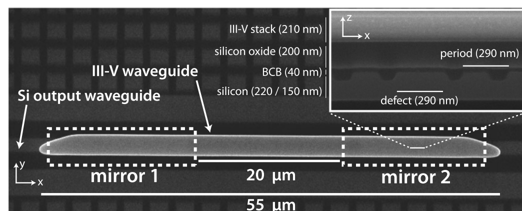

Fig. 2. Scanning electron microscope top-view image of a finished device. Inset, mirror cross section at grating defect.

defined by using contact lithography and inductively coupled plasma etching.

Figure 2 shows a top-view scanning electron microscope image of a finished device. The III–V waveguide masks the silicon cavities in the picture, but the white dashed boxes indicate the location and longitudinal extent of both silicon grating cavities. In this particular case, both mirrors are identical, and both have a silicon output waveguide. Each laser is 55 long and 2 μm wide. The dimensions of the III–V waveguide are chosen to facilitate fabrication through contact lithography. The silicon cavities each consist of 60 periods with a defect (quarter-wave shift) in the center. Although devices with different grating periods were fabricated, the grating period of this particular device is 285 nm, so each silicon cavity measures around 17 μm. The silicon cavities are spaced by 20 μm. The tapered edges of the III–V wire are intentionally patterned to avoid backreflection from the III–V waveguide facets. Both silicon output waveguides lead to a grating fiber-coupler. The inset in Fig. 2 is a focused ion beam cross section of one of the mirrors, showing the quarter-wavelength defect in the silicon grating.

The devices were measured at room temperature by illuminating each device individually from the top with an 800 nm distributed feedback pump laser. This pump laser was modulated to obtain 10 ns pulses with 10 mW peak power and a repetition rate of 1.5 μs. By use of an objective and a cylindrical lens, the shape of the illuminating spot was adjusted to match the shape of the III–V waveguide to be pumped. The output of the resonant-mirror laser is coupled to a silicon waveguide that guides it toward a grating coupler. From there, a cleaved fiber directs the laser output to a spectrometer equipped with a nitrogen cooled InGaAs line camera to measure the spectral power distribution of the laser output.

The laser output spectrum was measured for different values of the pump power, and the result is shown in Fig. 3. This graph clearly shows the intrinsic single-mode nature of this device: there is no competition between different longitudinal modes, not even at low pump power values, because the resonant mirrors are designed to reflect only one longitudinal laser mode. To obtain the relationship between the laser output power and the pump power (the light–light curve for optically pumped devices), the measured output spectra in Fig. 3 are integrated for each value of the pump power individually. The results are shown in the inset of Fig. 3. This graph very clearly shows the lasing threshold at 5.5 mW incident pump power. Assuming 30% power reflection at the InP–air interface and absorption coefficients of $3.3\ \mu\mathrm{m}^{-1}$ for InP and $4.47\ \mu\mathrm{m}^{-1}$ for InGaAsP, about

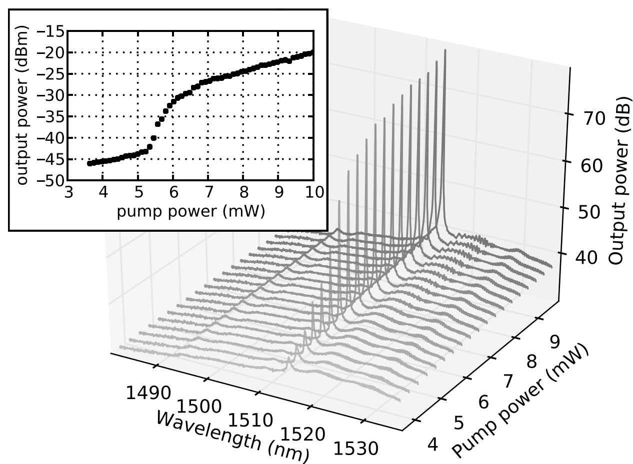

Fig. 3. Measured laser output-spectrum for different values of the pump power. Inset, laser output power in silicon waveguide as a function of the pump power ([9]; image courtesy of IEEE).

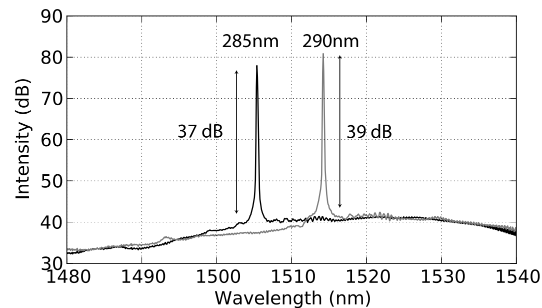

Fig. 4. Measured output spectrum of two different lasers: one with a 285 nm grating pitch and one with a 290 nm grating pitch ([9; image courtesy of IEEE]).

50% of the incident light will generate electron–hole pairs. This yields an upper limit for the device's actual threshold power of 2.6 mW. The laser peak output power in the silicon waveguide is conservatively estimated to be 10 μW, taking into account fiber-coupler efficiency. The duration of the pump pulse was increased and laser operation continued until a pulse duration of 1.2 μs (with a repetition rate of 1.5 μs, yielding an 80% duty cycle). CW operation is most likely hindered by self-heating, but this can be improved in future designs by optimizing the thermal impedance of the device. To investigate the spectral properties of the laser, consider Fig. 4. This graph shows the measured output spectrum for two different devices: one with a grating period of 285 nm and the other one with a grating period of 290 nm. Apart from the grating period, both devices are identical. This proves that the lasing wavelength is defined by the resonant wavelength in the silicon cavity. The side-mode suppression ratio is very high in both cases (37 and 39 dB, respectively). The lasing wavelength (1505 nm) of the device with a 285 nm grating period corresponds well to the peak reflectivity (1514 nm) of the 3D finite-difference time-domain simulation of the mirror in Fig. 1(b). The 9 nm deviation can be accounted for by small variations in the silicon thickness and grating etch depth. Electrical injection can be realized in future designs by adopting an injection scheme as proposed in [10]. This way the mode properties of the III–V waveguide can be engineered to match the properties of the design demonstrated in this work while also providing a path for electrical current. Alternatively an injection scheme similar to [11] can be used, provided the silicon cavities are fabricated in a thicker silicon layer to enable phase matching. The metal contacts and larger III–V mesa geometry necessary to realize electrical injection will also drastically improve the device's thermal impedance, paving the way for CW operation.

The authors acknowledge partial support from IWT through the SBO-Glucosens project as well as from ERC through the InSpectra project. Yannick De Koninck thanks the research foundation Flanders (FWO) for a research grant.

References

1. G. Roelkens, L. Liu, D. Liang, R. Jones, A. Fang, B. Koch, and J. Bowers, Laser Photon. Rev. **4**, 751 (2010).
2. S. Stankovic, R. Jones, M. N. Sysak, J. M. Heck, G. Roelkens, and D. van Thourhout, IEEE Photon. Technol. Lett. **24**, 2155 (2012).
3. Y. Halioua, A. Bazin, P. Monnier, T. J. Karle, G. Roelkens, I. Sagnes, R. Raj, and F. Raineri, Opt. Express **19**, 9221 (2011).
4. C. Sciancalepore, B. B. Bakir, X. Letartre, J. Harduin, N. Olivier, C. Seassal, J.-m. Fedeli, and P. Viktorovitch, IEEE Photon. Technol. Lett. **24**, 455 (2012).
5. Y. de Koninck, G. Roelkens, and R. Baets, IEEE Photon. J. **5**, 2700413 (2013).
6. H. A. Haus and Y. Lai, J. Lightwave Technol. **9**, 754 (1991).
7. K. Debnath, K. Welna, M. Ferrera, K. Deasy, D. G. Lidzey, and L. O'Faolain, Opt. Lett. **38**, 154 (2013).
8. ePIXfab: the silicon photonics platform (2012), http://www.epixfab.eu.
9. Y. de Koninck, F. Raineri, A. Bazin, R. Raj, G. Roelkens, and R. Baets, in *2012 IEEE Photonics Conference (IPC 2012)* (IEEE, 2012), pp. 1–2.
10. M. Tassaert, D. van Thourhout, and G. Roelkens, Opt. Quantum Electron. **44**, 683 (2012).
11. B. Ben Bakir, A. Descos, N. Olivier, D. Bordel, P. Grosse, E. Augendre, L. Fulbert, and J. M. Fedeli, Opt. Express **19**, 10317 (2011).